LARGE-EDDY SIMULATION OF A COMPRESSIBLE RIBBED CHANNEL FLOW

Gwenaël Hauët, Marcel Lesieur
L.E.G.I.,team MoST
BP 53
38041 Grenoble, France
hauet@hmg.inpg.fr,Marcel.Lesieur@hmg.inpg.fr

ABSTRACT

Past experimental and numerical studies have shown that the use of wall-mounted triangular streamwise ribs can lead to drag reduction. This phenomenon was intensively studied during the last twenty years, and DNS of Choi et al. (1993) provided very interesting explanations concerning the role of quasi-longitudinal vortices in the drag-reduction mechanism. This work concerned a flow of constant density above triangular riblets of high height. Large-eddy simulations (LES) have not been used a lot for these studies due to the complex geometry. Here, we employ the immersed boundary techniques proposed by Goldstein et al. (1995). On the upper plane (see Figure 1), an opposite force is imposed to model the riblets. We compare the influence of compressibility upon turbulent intensities of two sawtooth shape riblets. In the last part, we focus on the drag reduction mechanism in the subsonic case.

CONFIGURATION

We develop LES of a compressible channel flow. The simulations are carried out in the case of a periodic plane channel (see Figure 1). The size of the computational domain is $2\pi H \times \pi H \times 2H$, along the streamwise ($\hat{x}$ - U), spanwise ($\hat{y}$ - V) and normal ($\hat{z}$ - W) directions, respectively. The numerical simulations are carried out with a compressible Navier-Stokes solver that uses a fully-explicit McCormack scheme which is second-order accurate in time and fourth-order in space (Gottlieb et al., 1976)

$$\frac{\partial U}{\partial t} + \frac{\partial F_i}{\partial x_i} = S \tag{1}$$

where $U = (\rho, \rho u_1, \rho u_2, \rho u_3, \rho e)^T$, u_i is the velocity vector and e the total energy per mass unit. F_i are the fluxes in the three directions, and S is the source term. It allows in particular to keep the instantaneous mass flux constant.

$$S = (0, f(t), 0, 0, U_c f(t))^T \tag{2}$$

The numerical details can be found in Comte (1996).

Governing equations are non-dimensionalized by $U_c = 2\,U_b/3$ (where U_b is the bulk velocity assumed constant with time), the channel half-width H, the wall temperature, the viscosity at the wall, and the bulk density ρ_b (which is also constant). Let M_a be the Mach number, based on U_c and the sound speed at the wall. The subgrid-scale model used is the selective structure function model (Lesieur and Métais, 1996). In this model, the eddy viscosity ν_t is expressed in terms of the local second-order velocity structure function, and set to zero if the flow is not three-dimensional enough. The ratio of mean eddy to molecular viscosity is close to $\frac{\nu_t}{\nu} \simeq 1$. No Van Driest type damping of the eddy viscosity is made at the wall.

Table 1: Riblet configuration.

s/h	s^+	h^+
6.5	22	3
2	22	11

As already stressed, riblets are implemented with the aid of the immersed boundary technique (cf. Von Terzi et al., 2001; Goldstein et al., 1995; Lamballais and Silvestrini, 2002). The fluid feels the presence of a wall through the normal pressure force. A solid surface can be reproduced virtually thanks to an opposite external force. In the source term S of Eq. (2), we add the following virtual source:

$$S = (0, f_x, f_y, f_z, uf_x + vf_y + wf_z + g)^T \tag{3}$$

the velocity correction being

$$f_i = \alpha \int_0^t (\rho u_i(\vec{x}, t') - \rho u_i(\vec{x}, t')^S) dt' + \beta(\rho u_i(\vec{x}, t) - \rho u_i(\vec{x}, t)^S) \tag{4}$$

In the simple case of no-slip boundary conditions, the $u_i(\vec{x}, t)^S$ term is zero. The α and β parameters are equal to -4000 and 60 (values of Goldstein et al., 1998). Von Terzi et al. (2001) propose the following thermal correction in the compressible flow (low Mach number).

$$g = \alpha_t \int_0^t (T(\vec{x}, t') - T(\vec{x}, t')^S) dt' + \beta_t(T(\vec{x}, t) - T(\vec{x}, t)^S) \tag{5}$$

$T(\vec{x}, t)^S$ is the fixed wall temperature of the flat plane. The α_t and β_t parameters are of the order of 1 and -1, and depend slightly upon the Mach number. The flow is free behind the virtual surface. Its interaction with the real flow is not negligible. Many near-wall corrections exist (cf. Von Terzi et al., 2001). The surface recovered is so small in our case than the external force is also applied within the volume of the virtual riblets.

All the following simulations will be done at a *fixed* s, riblet spacing. We study two riblets with two different heights h. Table 1 shows riblet configuration. It is clear that the two Mach number considered ($M_a = 0.5$ and $M_a = 1.5$) modify slightly the wall Reynolds number. We will use the rounded value 170, computed on the flat wall. The computations were carried out for 500 and 960 non-dimensional time unit for subsonic and transonic cases respectively.

Validation. The code was satisfactorily validated at $M_a = 0.5$ against the uniform-density DNS of Choi et

al. (1993) for one configuration of riblets : $s^+ = 22$ and $h^+ = 11$. Choi et al. (1993) took 20 and 10 respectively (wall Reynolds number 180, computed on the flat plane). Figure 2 shows the friction coefficient and the rms streamwise velocity. Symbols are the DNS data. The latter profiles are displayed respectively above the riblet peaks and valleys in wall units. We use only eleven points along the riblet width. Our results are satisfactory despite the coarse resolution. The CPU time required for this case was about only 60 hours on the NEC-SX5. We lost a little bit of accuracy on the friction coefficient especially on the riblet peak, due to the geometric singularity.

RESULTS

Turbulence intensities

We first focus on the rms longitudinal velocity u', which is a good indicator of the longitudinal velocity streaks close to the wall. Figures 3 and 4 compare isolines of u' (both on the flat and ribbed walls) for two Mach numbers (subsonic $M_a = 0.5$, and "transonic" $M_a = 1.5$) and two riblet heights ($h^+ = 3$ and $h^+ = 11$). With the $h^+ = 3$ riblet, Walsh and Weinstein (1978) found experimentally in a wind tunnel at low Mach that there was a drag increase by a factor of the order of 2%. We obtain $0 \approx 2\%$ in the subsonic case, which is a good further validation of our LES code. In the transonic one, we find on the other hand for the low riblet that the drag is slightly *reduced* of $0 \approx 2\%$. In a constant-density drag-reduction configuration ($s^+ = 23$ and $h^+ = 9$), Goldstein et al. (1998) noted in their DNS that the rms longitudinal velocity has the same behaviour than for a flat wall with a shift up of about the riblet height. They observe also that the flow is slowed down in the riblet valleys, isovalues of u' being approximatively parallel above the ribs. This is obtained in our LES at $h^+ = 3$ in the transonic case (see Figure 4, left), as well as for the two other velocity components. It is clear that the difference observed between the subsonic flow at $h^+ = 3$ and the corresponding transonic flow comes from intense temperature gradients existing close to the walls. Notice that for $h^+ = 3$ and $h^+ = 11$, the high-intensity zone above riblets is more extended than above the flat plate, with a higher norm at $M_a = 1.5$. Indeed, let us assume as done by Choi et al. (1993) that the main role of riblets is to push the quasi-longitudinal vortices away from the wall. Since it is well known that compressibility straightens these vortices in the streamwise direction (Coleman et al., 1995, Lechner et al., 2001), then the effective surface of contact of vortices with riblets will be decreased with Mach number, and the drag decreased. This argument does not hold for high riblets, since vortices are already pushed very far away from the wall, with a small contact surface on the peaks (see Figures 3, right and 4, right). Let us mention also experiments of Coustols (2001) for high riblets ($s/h = 1$) with $s^+ > 20$ in a transsonic boundary layer where the drag is reduced of up to 2%.

About skin friction

All the following results refer to the subsonic case. At $h^+ = 11$, we have obtained a drag-reduction ratio of about 4% (cf. fig. 2). Figure 3 (right) shows isolines of u', with a flattening when h^+ is increased. In fact, the flow is more modified by riblets of low than high height, which may sound a little bit paradoxical. Figure 5 presents in this case ($h^+ = 3$ and 11) isosurfaces of Q (the second invariant of the velocity-gradient tensor) at a given positive threshold, which is well known to display properly coherent vortices (see e.g. Dubief et al., 2000). In both cases there is more small-scale turbulence on the ribbed-wall side. We see indeed at $h^+ = 3$ a stronger asymmetry in the quasi-longitudinal vortex system between the flat and ribbed walls. For $h^+ = 11$, the longitudinal vortices are just shifted away from the wall, as observed already by Choi et al. (1993). It is well known from the work of Choi et al. (1993) that, in order to achieve drag reduction, s^+ should be smaller than the average diameter (≈ 25) of quasi-longitudinal vortices.

Figure 8 is reproduced Choi et al. (1993), with grey zones representing regions of higher friction. Their areas are much larger for $s^+ = 40$ (the drag-increasing case).

Figure 6 present a vertical cross section of instantaneous longitudinal vorticity for the two riblets. On the top, only the appearance of small-scale vortices does reveal the presence of riblets. On the other hand, one sees on the bottom and as already stressed a shift of the flat-wall boundary-layer longitudinal-vortex system. A zoom in the middle of the domain is presented on figure 7. For $h^+ = 3$, a configuration of drag increase, vortices stick along the "wet" surface and penetrate into the valleys. For $h^+ = 11$, the wet surface is reduced to the riblet peaks.

In the transonic case, the vortex topology is approximately the same.

ACKNOWLEDGEMENTS

The computations were carried out at the " Institut du Développement et des Ressources en Informatique Scientifique".

REFERENCES

Choi, H., Moin, P., and Kim, J., 1993, "Direct numerical simulation of turbulent flow over riblets", *Journal of Fluid Mechanics*, Vol. 255, pp. 503-539.

Coleman, G.N., Kim, J., and Moser, R.D., 1995, "A numerical study of turbulent supersonic isothermal-wall channel flow", *Journal of Fluid Mechanics*, Vol. 305, pp. 159-183.

Comte, P., 1996, "Numerical methods for compressible flow", in *Computational Fluids Dynamics*, Les Houches; session *LIX*, 1993 Lesieur, Comte, Zin-Justin eds., Elsevier Sciences Publishers, 1996.

Coustols, E., 2001, "Effet des parois rainurées (<<riblets>>) sur la structure d'une couche limite turbulente", *Mécanique et Industrie* , Vol. 2, pp. 421-434.

Dubief, Y. and Delcayre, F., 2000, "On coherent-vortex identification in turbulence", *Journal of Turbulence*, Vol. 1.

Goldstein, D., Handler, R., and Sirovich, L., 1995, "Direct numerical simulation of turbulent flow over a modelled riblet covered surface", *Journal of Fluid Mechanics*, Vol. 302, pp. 333-376.

Gottlieb, D., and Turkel, E., 1976, "Dissipative two-four methods for time-dependent problems", *Mathematical Computation*, pp. 703-723.

Lamballais,E. and Silvestrini, J.H., 2002, "Direct Numerical Simulation of interactions between a mixing layer and a wake around a cylinder", *Journal of Turbulence*, Vol. 3.

Lechner, R., Sesterhenn, J., and Friedrich, R., 2001, "Turbulent supersonic channel flow", *Journal of Turbulence*, Vol. 2.

Lesieur, M., and Métais, O., 1996, "New trends in large-eddy simulations of turbulence", *Annual Review of Fluid*

Mechanics, Vol. 28, pp. 45-82.

Von Terzi, D. A., Linnick, M. N., Seidel, J., and Fasel, H. F., 2001, "Immersed boundary techniques for high-order finite-difference methods", *AIAA Paper*, A01-2918.

Walsh, M. J., and Weinstein, L. M., 1978, "Drag and heat transfer on surfaces with small longitudinal fins", *AIAA Paper*, A78-1161.

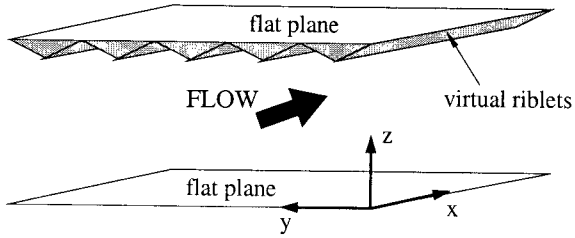

Figure 1: Computational domain

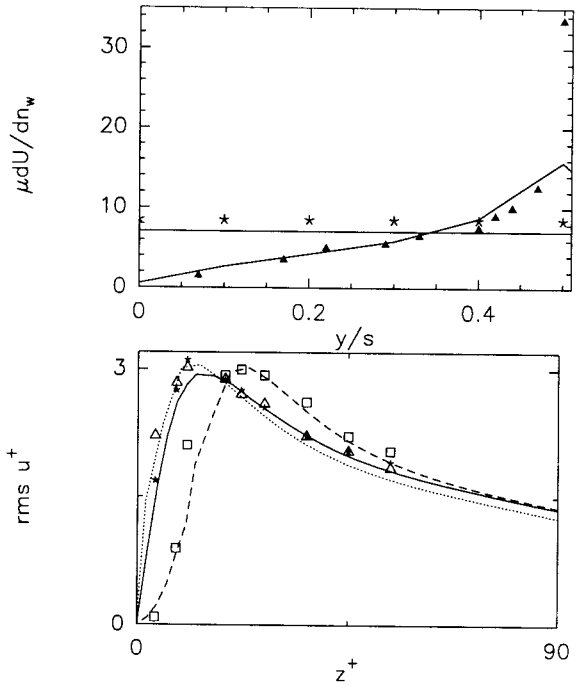

Figure 2: LES at $M_a = 0.5$ with the higher riblet. Comparaison of friction coefficient (top) and rms longitudinal velocity in wall units (bottom) against Choi et al.'s (1993) numerical data. Lines (LES): straight (flat plane), dashed (peaks), dotted (valleys); symbols (DNS): star (flat plane), triangle (peaks), square (valleys).

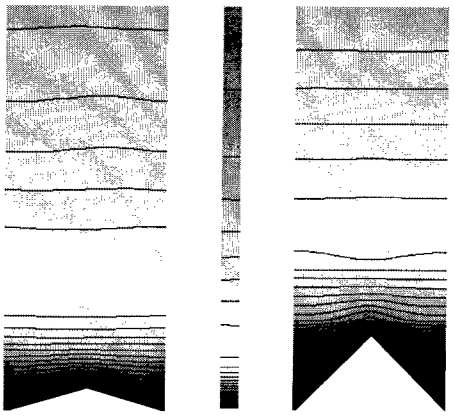

Figure 3: Isovalues of rms streamwise velocity in global coordinates on the flat and ribbed wall in the subsonic flow. From left to right: $h^+ = 3$, flat wall, $h^+ = 11$.

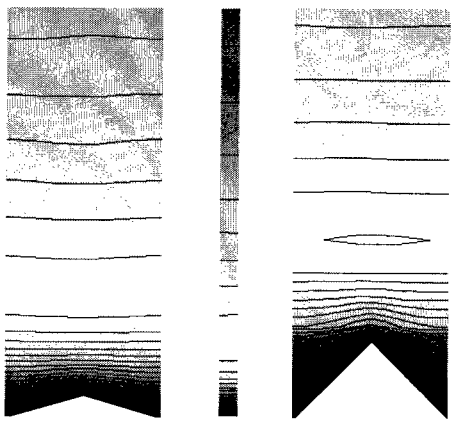

Figure 4: Isovalues of rms streamwise velocity in global coordinates on the flat and ribbed wall in the transonic flow. From left to right: $h^+ = 3$, flat wall, $h^+ = 11$.

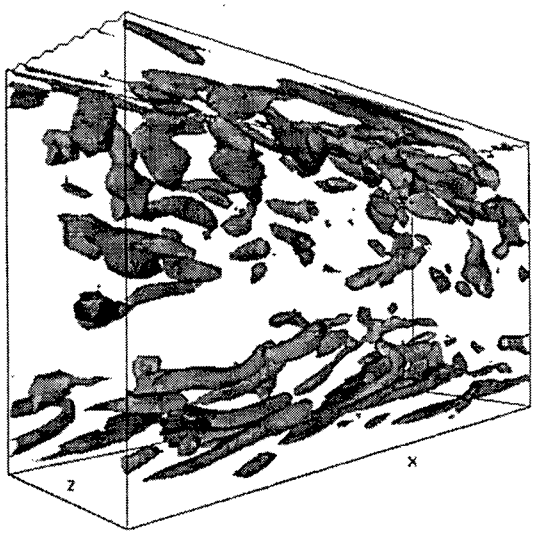

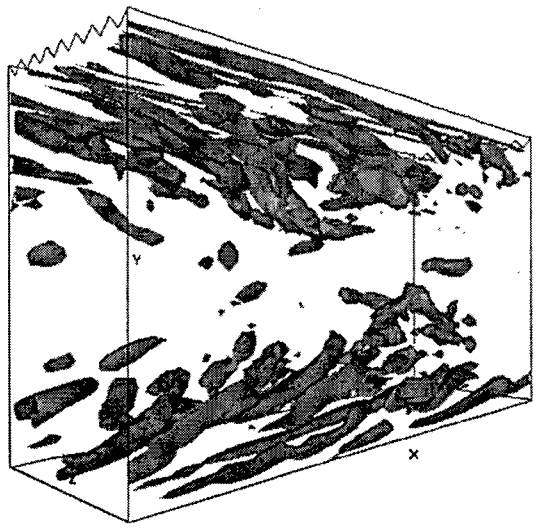

Figure 5: Isosurfaces of instantaneous Q criterion ($Q = 0.08$) for the subsonic ribbed channel flow with two heights of riblets: on the top $h^+ = 3$, on the bottom $h^+ = 11$.

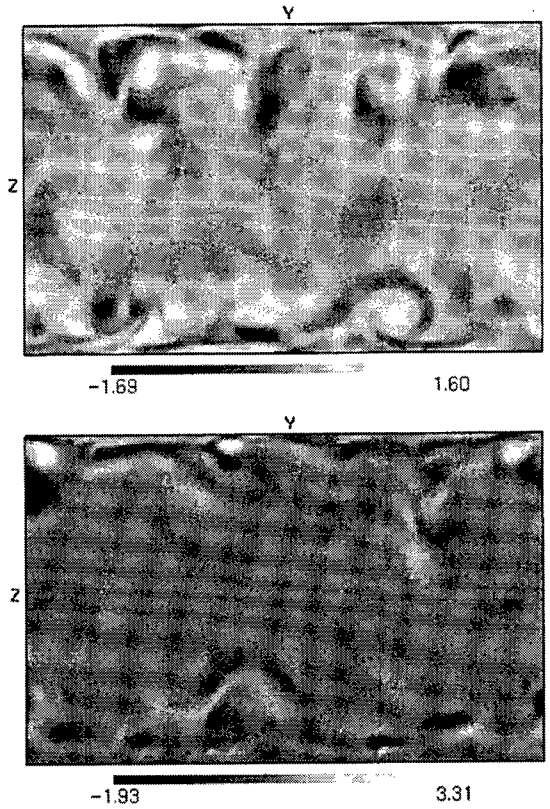

Figure 6: Cross section of instantaneous streamwise vorticity in the subsonic case: top $h^+ = 3$, bottom $h^+ = 11$.

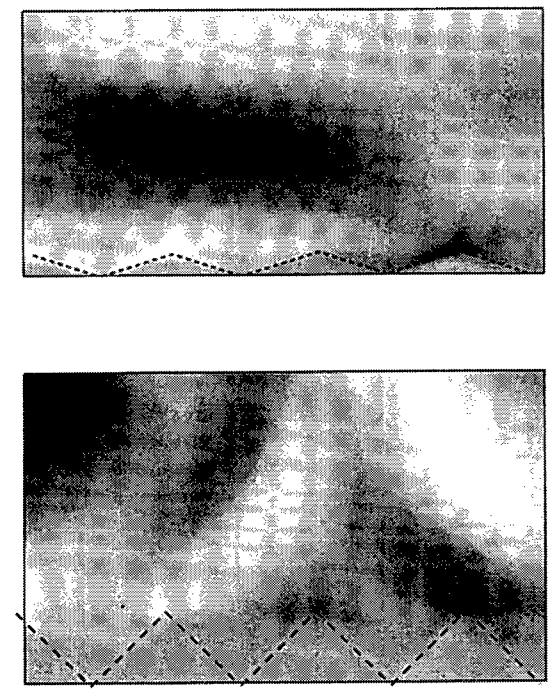

Figure 7: Zoom of the last figure.

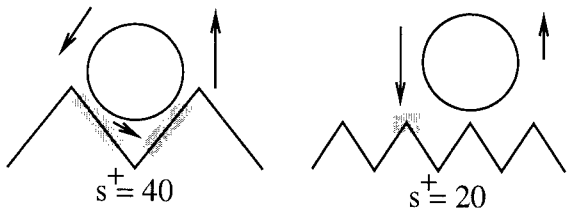

Figure 8: Schematic diagram of drag increase and reduction mechanisms by Choi et al. (1993).